Journal of Materials Chemistry A

Accepted Manuscript

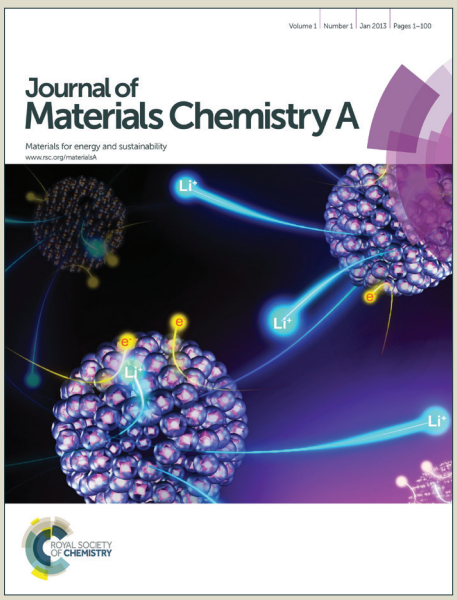

ROYAL SOCIETY OF CHEMISTRY

www.rsc.org/materialsA

Journal of Materials Chemistry A RSCPublishing

ARTICLE

Interface layer formation in solid polymer electrolyte lithium batteries: an XPS study

Cite this: DOI: 10.1039/x0xx00000x

Chao Xu, Bing Sun, Torbjörn Gustafsson, Kristina Edström, Daniel Brandell* and Maria Hahlin

Received ooth January 2012,
Accepted ooth January 2012

DOI: 10.1039/x0xx00000x

www.rsc.org/

The first characterization studies of the interface layer formed between a Li-ion battery electrode and a solid polymer electrolyte (SPE) are presented here. SPEs are well known for their electrochemical stability and excellent safety, and thus considered good alternatives to conventional liquid/gel electrolytes in high-energy density battery devices. This work comprises studies of solid electrolyte interphase (SEI) formation in SPE-based graphite|Li cells using X-ray photoelectron spectroscopy (XPS). SPEs based on high molecular weight poly(ethylene oxide) (PEO) and lithium bis(trifluoromethanesulfonyl) imide (LiTFSI) salt are studied. Large amounts of LiOH are observed, and the XPS results indicate a correlation with moisture contaminations in the SPEs. The water contents are quantitatively determined to be in the range of hundreds of ppm in the pure PEO as well as in the polymer electrolytes, which are prepared with a conventional SPE preparation method using different batches of PEO and different drying temperatures. Moreover, severe salt degradation is observed at the graphite/SPE interface after the 1st discharge, while the salt is found to be more stable at the Li/SPE interface or when using LiTFSI-based liquid electrolyte equivalents.

Introduction

Since their commercialization in 1991 by the Sony Corporation, rechargeable lithium ion batteries (LIBs) have been widely utilized as power sources for portable electronic devices. They are also considered as the most promising candidates for energy storage systems and power supply in hybrid electric vehicles (HEVs), electric vehicles (EVs) and plug-in hybrid electric vehicles (PHEVs).[1,2]

With respect to safety and ageing, one of the most critical components in the LIB is the electrolyte. Conventionally, today's commercial batteries utilize liquid electrolytes based on lithium salt dissolved in low molecular weight organic carbonates. However, the electrochemical instability and potential leakage of these flammable organic solvents will be serious safety hazards for up-scaled lithium-ion cells.[3] In this context, a LIB based on a solid polymer electrolyte (SPE), which acts as both separator and ion conduction medium, would possess better chemical stability and display enhanced safety as compared to batteries based on liquid electrolytes.[4,5] Moreover, SPEs could preferably be used in elevated temperature LIB applications due to much better thermal stability and safety than obtained with conventional liquid electrolytes.[4–6] A well-known drawback in SPEs – generally based on polyethers, such as poly(ethylene oxide) (PEO) – is that they suffer from relatively low ionic conductivity at ambient temperatures. Several approaches have been investigated to improve the ionic conductivity of polymer electrolytes, for instance the addition of metal oxides nanoparticles[7–10] or plasticizers.[11,12] Polymer modifications such as cross-linking, copolymerization and functionalization have also been promising strategies for performance improvement.[13–18] Alternatively, new polymer host materials, such as polycarbonates, have been considered.[19,20]

One essential concept for understanding of LIB operation is the solid electrolyte interface (SEI), which is a passivating layer formed on the electrodes – mainly on the anode surface – primarily during the first cycle.[21] SEI layer formation at the electrode/electrolyte interface originates from the mismatch between the electrochemical stability window (i.e., oxidation/reduction limits) of the electrolyte and the electrochemical potential of the electrodes.[22] The SEI comprises components that are usually products from salt degradation and solvent reduction in the electrolyte.[23–25] The performance of LIBs, for example rate capability, reversible capacity and safety, is greatly influenced by the stability and composition of the SEI layer.[26] A stable passivating SEI layer protects the electrode from further reaction with the electrolyte, thereby avoiding undesired electrolyte consumption, but also limits the kinetics of the ion transport processes. Moreover, most of the compounds in the SEI layer contain Li, associated with an irreversible capacity loss. Therefore, understanding the formation mechanism as well as the chemical composition of the SEI is crucial for battery performance improvement.

Analyzing pristine SEI layers constitutes significant challenges due to the technical difficulty in characterizing nano-meter scale layers at the individual electrode/electrolyte interfaces. Moreover, most of the components of the SEI layer are highly sensitive to air, moisture and other external contaminants, which make characterization and interpretation difficult.

Nevertheless, a lot of research has been devoted to this area and a variety of techniques have been used for analysis.[27–32] In this context, photoelectron spectroscopy is one of the most widely used techniques for surface analysis due to its extraordinarily high surface sensitivity, and has also been widely used when characterizing the SEI layer for conventional liquid electrolytes.[24,26,33] The surface sensitivity of X-ray photoelectron spectroscopy (XPS) corresponds well to the thickness of the SEI in the conventional Li-ion battery, making this technique particularly suited for studying the interfacial chemistry in batteries.[26]

Due to the rapidly growing interests in using intrinsically safe electrolytes such as SPEs in LIBs for large-scale applications (e.g., HEV/EVs), a better understanding of the electrolyte/electrode interface chemistry in SPE based LIBs is urgently needed.

So far, little effort has been devoted into SEI characterization in SPE-based batteries. Peled et al. could detect SEI layer formation on the lithium surface in composite polymer electrolyte batteries based on EIS results, but the technique did not allow analysis of its composition.[34,35] Le Granvalet-Mancini et al. studied the passivation layer formed on the lithium metal which is in contact with PEO-triflate SPE using Atomic Force Microscopy (AFM) and concluded that the layer has low conductivity.[36] Ismail et al. used XPS to investigate the surface layer on lithium metal after contact with lithium salt doped SPEs. The formed layer was found consisting of the salt decomposition product LiF together with the native film compounds Li_2CO_3/LiOH and Li_2O, which existed on the as-received lithium metal.[37] To the best of our knowledge, no analysis of the SEI layer formed in graphite-based LIBs using SPEs has yet been presented.

To investigate whether or not there is an SEI formed during battery operation, and if so, what is its composition, we have here taken the initiative using XPS to investigate the interface chemical composition in SPE-based graphite half-cells (i.e., towards Li metal). An SPE consisting of high molecular weight PEO and LiTFSI was chosen as a standard SPE system. A practical difficulty when analyzing SPE-based LIB systems is acquiring useful surfaces for measurements after battery disassembly due to the electrode particle adhesion to the polymer. This requires a compromise between achieving useful electrochemical performance, corresponding to good interfacial contacts, and the possibility to separate the electrode and SPE apart for XPS analysis after electrochemical cycling. Therefore, we have chosen to operate the batteries at 50 °C to achieve acceptable electrochemical performance (above room temperature) but also to be able to disassemble the cells (below the PEO melting temperature at ~65 °C). For comparison, an LIB using a liquid electrolyte operated at the same temperature with the same electrolyte salt has also been investigated. Furthermore, since PEO is hygroscopic, the effect of different water contents in the polymer electrolyte on the SEI composition has also been investigated.

Experimental

Electrolyte, electrode and battery preparation

Lithium bis(trifluoromethanesulfonyl)imide (LiTFSI, Ferro) salt was vacuum-dried at 120 °C for 24 hours prior to use. Two batches of poly(ethylene oxide) (PEO, Mw=4,000,000), produced by Aldrich and BDH Chemicals LtD Poole England, were both dried at two different temperatures, 50 °C for 72 hours and 120 °C for 24 hours under vacuum, respectively. SPE samples were prepared by dissolving 471.9 mg PEO (dried at 120 °C, Aldrich) and 123.0 mg LiTFSI in 2 mL acetonitrile (anhydrous, 99.8 %, Sigma-Aldrich; further dehydrated with 3 Å molecular sieves, Merck). Constant molar ratio of ether oxygen unit to salt (25:1) was used and is referred to as PEO_{25}LiTFSI. After being stirred at 50 °C over-night in the glove box, the mixture was casted on a Teflon plate. The plate was then placed into two different drying setups in an Argon-filled glove box (O_2 < 2 ppm, H_2O < 1 ppm); one using a setup by sealing the plate in an air-tight polyethylene-coated aluminum bag ('soft-bag') similar to a battery pouch cell and the other is a container designed to better prevent moisture contamination during the drying process, consisting of a cuboid-shaped stainless steel container with a removable lid for sample holder transfer and two valves for gas flow control. A rubber ring was placed between the lid and the container for tight sealing. The PEO used for both SPE samples, which were prepared by the described two setups respectively, were produced by Aldrich. The 72 hours at 50°C vacuum-dried PEO was utilized for the SPE which was prepared with 'soft-bag' setup and the 24 hours at 120 °C vacuum-dried one was used with 'designed container'. As conventionally for SPE drying, both setups were connected to an external dry N_2 flow to remove the solvent at room temperature for 72 hours. Two needles were inserted into the 'soft-bag' in order to introduce N_2 flow. For comparative studies, 1M LiTFSI salt dissolved in ethylene carbonate (EC) and diethylene carbonate (DEC) (2:1) was used in a liquid electrolyte-based cell.

Graphite electrodes were prepared by coating a slurry of graphite (Graphit Kropfmühl AG), super-P carbon black (Erachem Comilog), TIMREX® KS-6 graphite (TIMCAL) and Kynar 2801® (Handlapp) with a mass ratio of 85:3:2:10 onto copper foil. The slurry was mixed by ball milling for one hour and casted on a Cu foil using doctor-blading. The electrodes were punched with a diameter of 12 mm and dried under vacuum at 120 °C for 12 hours. The obtained mass loading of the active graphite was 2.04 mg/cm^2

For cell assembly, graphite|polymer electrolyte|Li half-cells were prepared inside an Ar glovebox by sandwiching a self-standing PEO_{25}LiTFSI membrane between two electrodes and vacuum-sealing the cells in a 'coffee-bag' design. Lithium foil was produced by CYPRUS Foote Mineral Co. and used as received. For the liquid electrolyte cell, a Solupor polymer separator soaked with liquid electrolyte was used.

Measurements

The electrochemical performance of the LIBs was characterized galvanostatically at 50 °C using a Digatron BTS battery testing system outside the glovebox for both liquid and polymer electrolyte batteries at a discharge rate C/50. SPE based half-cells were preheated at 50 °C for 12 hours prior to cycling to promote interfacial contacts. The battery discharge was cut off at 0.01 V vs. Li^+/Li for the first discharge.

Karl-Fischer titration on a 756 KF Coulometer (Metrohm) was used to measure the water content in the samples. All measurements were performed within an Ar glovebox to prevent risks of moisture contaminations. Samples were prepared by dissolving SPEs in a measured weight of acetonitrile and the solution was stirred over-night before each measurement. By determining the water content in the acetonitrile and the SPE dissolved solution, respectively, the exact water content in the SPE can be computed.

XPS measurements were performed on a PHI 5500 system with monochromatized AlKα radiation (hν = 1487 eV) as light source. The samples were prepared by carefully disassembling the cycled batteries in an Ar filled glove box and then transfer them to the spectrometer with an appropriately designed transfer chamber to avoid moisture and air contamination. For the liquid electrolyte based battery, the lithium and graphite surfaces were washed with dimethyl carbonate (DMC) before sample transfer. The obtained spectra were curve fitted by Igor software (version 4.0.7), using mixtures of Gaussian and Lorentzian line shapes (Lorentzian FWHM were kept lower than 0.1 eV). The S2p spin-orbit splitting energy value used in this work for curve fitting was 1.2 eV. The peaks were calibrated versus the C1s peak of hydrocarbon species at 285 eV. The relative surface concentration was calculated as $C_x=(A_x/\sigma_x)/\Sigma(A_y/\sigma_y)$, where A is the intensity and σ is the sensitivity factor given by the Multipak software (version 6.1A). The obtained concentration was based on a uniform distribution of elements. Electron neutralizer was applied when measuring SPE samples.

Results and discussion

Water content measurements - Karl Fischer titration

Moisture is an undesirable substance in conventional liquid electrolyte LIBs because it causes degradation of battery components and affects battery performance; especially in $LiPF_6$-based systems.[38,39] The most widely studied polymer host matrix for SPEs is PEO, which is a hygroscopic material. As such, it is difficult to remove absorbed water from pristine PEO and keep the moisture level of PEO-based polymer electrolyte LIBs as low as for liquid electrolytes.

Table 1. Karl-Fischer titration measurement results for acetonitrile (ACN) solvent, poly(ethylene oxide) and prepared polymer electrolyte: $PEO_{25}LiTFSI$.

	ACN	PEO (Aldrich)		PEO(BDH)	
		50 °C	120 °C	50 °C	120 °C
Water content (ppm)	5	690	142	150	86
	$PEO_{25}LiTFSI$ (dried with different setups)				
	Designed container			Soft-bag	
Water content (ppm)	675			2300	

Elevated drying temperatures of 120 °C have been used in order to reduce absorbed water in the pristine PEO as much as possible. Table 1 shows the results of the water content determination for the various compounds used for the following experiments in this work (LiTFSI in CAN giving the same amount as the pure solvent). As expected, the results indicate that the water content in the PEO dried at 120 °C (142 ppm) is much lower than the 50 °C dried sample (690 ppm). This was further confirmed by testing another batch of PEO with the same molecular weight but from a different producer (BDH Chemicals LtD). The water contents in this batch for 50 °C and 120 °C dried samples were 150 ppm and 86 ppm, respectively. The results indicate obvious differences in water levels between the batches, especially for the samples dried at 50 °C. This indicates that the water content in PEO can vary significantly for different batches. Water contents in the range of hundreds of ppm implies that even without any further moisture contamination during the following SPE casting processes, the water content for the as-prepared PEO-based SPE will be much higher than in conventional liquid electrolyte (below 10 ppm). This was also confirmed by the Karl-Fischer titration results of the as-prepared SPEs prepared with different setups; see Table 1. The sample dried within the custom-fit designed container, which has a better sealing ability, has 675 ppm water, while the sample using a soft-bag setup has as high water content as 2300 ppm. The high water level is most likely due to the moisture contamination from air, since the sealing in the soft-bag setup was not as good as in the designed container. This relatively high water level shows good agreement with previous studies of water contents in PEO-based SPEs,[40,41] and can well be a general property for this class of materials.
The SPEs with different moisture contents (675 ppm and 2300 ppm) were selected for battery assembly and further investigated by electrochemical characterization together with XPS measurements to study the difference in interfacial chemistry in comparison with one liquid electrolyte battery.

Electrochemical characterization

The first discharge curves for the three batteries studied with XPS are shown in Figure 1. All cells were cycled at 50 °C at a C/50 rate. Additionally, the polymer electrolyte batteries had been pre-heated at 50 °C for 12 hours in order to improve the contacts between the SPE and the electrodes. The reason for discharging at such a low rate (C/50) is to ensure that the electrochemical reaction can occur in the SPE batteries despite the poor initial contact between the SPE and the electrode, and also that the ionic conductivity of the SPE is not a limiting factor.

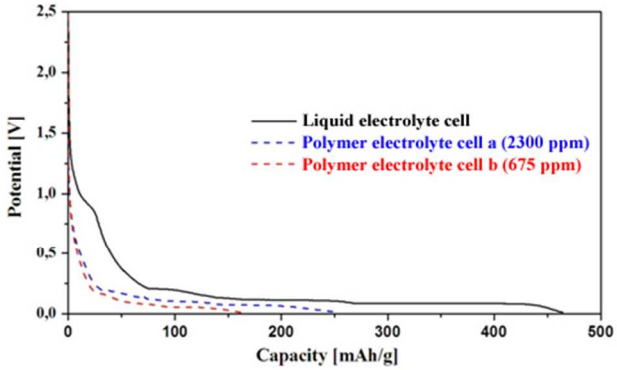

Figure 1. The first discharge curves for the liquid electrolyte (1M LiTFSI in EC:DEC=2:1) cell (solid black) and the two polymer electrolyte cells with different moisture contents (dashed blue and red lines).

The plateau at 0.8-0.9 V in the first discharge curve for the liquid electrolyte battery is well-known and related to the SEI layer formation.[24] However, for the polymer electrolyte batteries a and b, the region (1.0-0.2 V) before the intercalation plateaus shows a steadily declining slope, indicating that the conventional SEI layer is not formed. In this context, it should be noted that the electrochemical stability window of any electrolyte – SPE or liquid – is critical for the SEI formation. For the LiTFSI-PEO SPEs investigated here, the stability window has previously been determined to be 0.5 V to 4 V vs.

Li^+/Li.[5] Therefore, an SEI layer is still expected to be formed when the battery is discharged to 0.01 V, but different from the SEI layer formed in conventional liquid electrolyte systems which are mainly products form the reduction of organic solvents at higher potentials (e.g. ~1.3 V vs. Li^+/Li for DEC, ~0.9 V vs. Li^+/Li for EC).[42]

The gravimetric capacities achieved for the liquid electrolyte battery and the polymer electrolyte batteries a and b are 463, 250 and 160 mAh/g, respectively. The obtained capacity for the liquid electrolyte battery is larger than theoretical capacity 372 mAh/g, which can be attributed to the SEI formation during the first discharge. The capacity of the two SPE-based graphite half-cells was found to be lower than the liquid electrolyte cell. This can perhaps be attributed to the low ionic conductivity of the SPEs, but primarily to the poor wetting between the SPE and the electrode active material particles. Although neither of the two SPE batteries reaches the theoretical capacity, the one with higher water content (2300 ppm) displayed higher capacity than the one with lower water content (675 ppm). This could be due to better adhesion of the SPE to the electrodes at higher water contents, caused by improved wetting. Another possibility is that an increased amount of water enhances the ionic conductivity of the SPE, giving rise to less mass transport limitations.

XPS studies

The graphite/SPE interface. Adhesion of the polymer electrolyte to both the positive and negative electrodes was apparent upon disassembling the discharged batteries. However, successful disassembly with reasonably clean sample surfaces can still be obtained using controlled battery operation temperature (50°C) and careful disassembly. To investigate the chemical processes occurring in the interface region between the polymer electrolyte and both electrodes, both sides of each interface were probed. For each polymer electrolyte battery, this results in four samples: the graphite electrode, the polymer surface facing graphite electrode (hereafter called as PEO(G)), the polymer electrolyte surface facing the Li foil (called as PEO(Li)) and the Li electrode. Figure 2 shows the F1s, O1s, N1s, C1s, and S2p spectra of the samples related to the SEI formation at the graphite side of the batteries. The samples are going from top to bottom 1) pristine graphite, 2) pristine SPE, 3-6) graphite and SPE surfaces from SPE-based graphite half-cells after 1st discharge (middle four) with high (3-4) and low (5-6) H_2O contents, and 7) the graphite electrode from the liquid electrolyte graphite half-cell after 1st discharge. The relative surface concentrations of the elements in these surfaces are given in Table 2.

The sharp peak with highest intensity at a binding energy of 284.5 eV in the C1s spectrum for pristine graphite electrode is corresponding to the presence of graphite as well as amorphous carbon black. The signal of the Kynar 2801® binder can be found at 286.3 eV, 288.6 eV, 290.8 eV and 293.4 eV in the C1s spectrum as well as at 687.8 eV and 689.6 eV in the F1s spectrum. In ex-situ prepared samples, very small amount of O contamination can always be detected on the pristine graphite electrode, which to some extent may explain the low signal-to-noise ratio in the O1s spectra of the pristine graphite sample. This is further confirmed by the low surface atomic concentration of O seen in Table 2. For the pristine PEO_{25}LiTFSI sample, the C1s peak at 286.6 is attributed to PEO while the O1s peak at 533 eV contains an overlap with the signals from the ether oxygen of PEO, oxygen from the salt anions and water oxygen. The F1s peak at 688.9 eV, C1s peak at 292.9 eV, $S2p_{3/2}$ peak at 168.9 eV and N1s peak at 399.7 eV all correspond to the salt LiTFSI salt. In the S2p spectra, small amounts of other sulfur-containing species can be found in the pristine sample, seen as two additional S2p signals at binding energies of 167.5 eV and 163.7 eV. This feature is commonly seen in SEI studies on LiTFSI salt-based LIBs.[31,32,43]

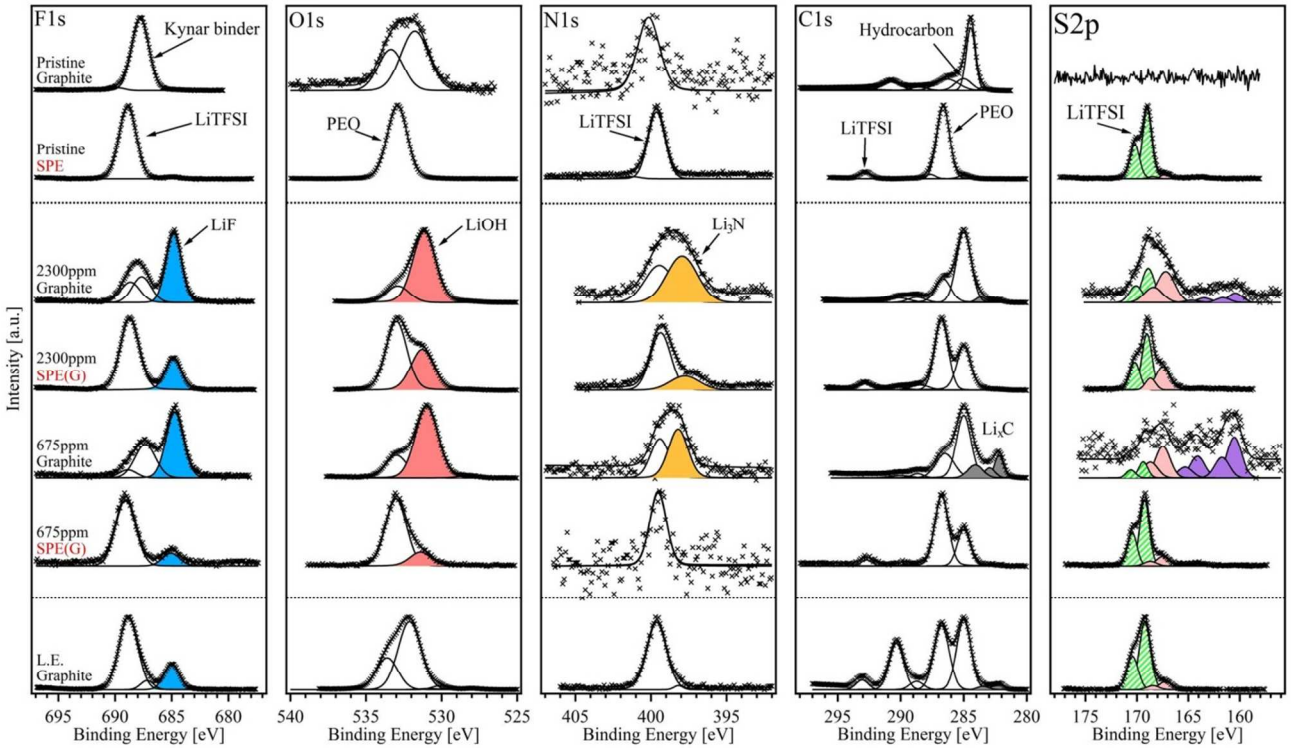

Figure 2. F1s, O1s, N1s, C1s, S2p spectra of (from top to bottom) pristine graphite, SPE, graphite and SPE(G) from SPE-based graphite half-cells with high and low H_2O content, and of a graphite electrode from a liquid electrolyte (L.E.) battery. Highlighted with difference colors are: LiF (blue), LiOH (red), Li_3N (yellow), Li_xC (grey), LiTFSI (green-patterned), Li_2SO_3 (pink), and polysulfur and Li_2S (purple).

Table 2. Relative surface concentrations of F, O, N, C, S and Li in pristine graphite, SPE, graphite and SPE(G) from both SPE-based graphite half-cells and a graphite electrode from liquid electrolyte battery.

	F	O	N	C	S	Li
Graphite	12.08	2.48	0.90	84.54	0.00	0.00
SPE	12.94	30.38	1.61	47.68	3.29	4.01
Graphite (2300 ppm)	6.48	29.70	1.16	43.77	0.58	18.31
SPE(G) (2300 ppm)	10.59	27.64	1.65	41.15	2.82	16.15
Graphite (675 ppm)	7.69	20.18	1.85	55.66	0.34	14.28
SPE(G) (675 ppm)	11.76	26.82	3.17	46.82	2.44	8.99
Graphite (L.E.)	9.83	33.56	1.17	36.29	1.74	17.41

Despite the adhesion between the polymer electrolyte and the electrodes, the separation of the parts was apparently successful since only small amounts of SPE residues can be observed on the graphite electrodes. This is seen primarily by the low intensity ratio between the characteristic C1s PEO peak (286.6 eV) and that of the total C1s intensity, and the O1s PEO (533 eV) and the total O1s intensity, for the electrode samples after 1st discharge. However, the relatively low graphite signal clearly shows that there is an interfacial layer formed on the electrode. The differences in relative peak intensities in the spectra show that the formed interphases have different composition as compared to the polymer electrolyte. All the surfaces from the SPE-based graphite half cells contain the LiTFSI salt, as seen by the presence of the F1s peaks at 688.8 eV, the N1s peaks at 399.7 eV and the S2p peaks at 169 eV. Another common feature for all interface samples is the presence of a peak at a binding energy of 685 eV in the F1s spectra, which corresponds to formation of LiF. This LiF may originate from either binder and/or salt decomposition since both the binder Kynar 2801® and LiTFSI salt contain F.

Besides the formation of LiF at the graphite/SPE interface, several other new interface components can be observed in the XPS results. The formed interface layers are found to be almost identical in composition for the two SPEs used in the SPE-based graphite half-cells, although the water contents are substantially different. The strong O1s signals at 513 eV on both graphite and SPE(G) surfaces for both 2300 ppm and 675 ppm SPE batteries are attributed to LiOH. LiOH is not a common compound for conventional SEI layers formed in liquid electrolyte based LIBs since the major LiOH producing reaction probably is Li^+ reacting with H_2O,[44] and the water content in liquid electrolyte is generally kept at very low level (only a few ppm). Thus, the high water content in the SPEs has a critical influence on the interface layer produced on graphite during battery cycling.

The relative amounts of LiOH at the two SEIs are found to be 81.2% for 2300 ppm SPE battery and 77.6% for 675 ppm battery (of the total O atom signals). Besides LiOH, hydrocarbon species are clearly formed at this interface, seen from the strong signal at 285 eV in the C1s spectra of both graphite and SPE(G) surfaces from both SPE batteries. Various kinds of carbon species can be the source, such as PEO, binder, graphite, etc – this is commonly found also for liquid electrolyte systems, but could here indicate PEO decomposition. Furthermore, C and O are found to be the two elements with highest concentrations according to Table 2. In summary, the SEIs formed at graphite surfaces are dominated by LiOH and hydrocarbon species.

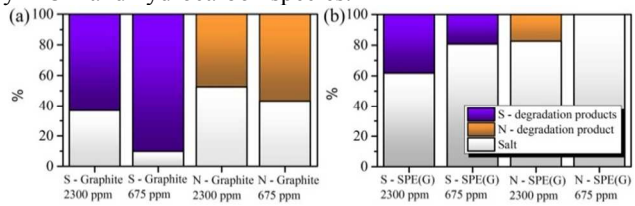

Figure 3. Relative atomic percentage of S- and N-containing compounds on the surfaces of (a) the graphite electrodes and (b) the SPE(G)s from the two SPE graphite half-cells.

Moreover, the $TFSI^-$ anion experienced significant degradation during the first discharge process in the SPE graphite half-cell at the graphite-SPE interface. This phenomenon has been addressed in previous studies suggesting possible decomposition reactions for various anions (e.g., $CF_3SO_3^-$ and ClO_4^-) in PEO-based SPEs, which undergo reductive cleavage to form radicals.[45,46] M. Nakayama et al. also observed $TFSI^-$ anion decomposition in a $LiFePO_4$|SPE|Li cell using *in situ* NMR imaging technique.[47]

According to both the S2p spectra from graphite and the atomic percentage values in Figure 3(a), the amount of salt degradation products formed on the graphite surfaces corresponds quantitatively to the amount of pristine salt found. Based on the binding energy position, the degradation product is suggested to be Li_2SO_3[48] ($S2p_{3/2}$ peak at 167.4 eV, pink doublets; Figure 2). Salt degradation is also observed in the N1s spectra, in which a new peak appears at a lower binding energy of 397.5 eV. This peak is assigned to be Li_3N since this region is usually attributed to metal nitrides. Apart from Li_2O formation, which has not been detected in this study, these discoveries fit well with the suggested LiTFSI degradation mechanism:[49]

$$\mathrm{LiN(SO_2CF_3)_2} + \mathrm{ne^-} + \mathrm{nLi^+} \rightarrow \mathrm{Li_3N} + \mathrm{Li_2S_2O_4} + \mathrm{LiF} + \mathrm{C_2F_xLi_y}$$

$$\mathrm{LiN(SO_2CF_3)_2^-} + \mathrm{2e^-} + \mathrm{2Li^+} \rightarrow \mathrm{Li_2NSO_2CF_3} + \mathrm{LiSO_2CF_3}$$

$$\mathrm{Li_2S_2O_4} + \mathrm{6e^-} + \mathrm{6Li^+} \rightarrow \mathrm{2Li_2S} + \mathrm{4Li_2O}$$

$$\mathrm{Li_2S_2O_4} + \mathrm{4e^-} + \mathrm{4Li^+} \rightarrow \mathrm{Li_2SO_3} + \mathrm{Li_2S} + \mathrm{Li_2O}$$

The absence of Li_2O in this study may be attributed to the relatively high water content in the SPEs, since Li_2O can react with H_2O through hydrolysis. Interestingly, Li_2S, which can also hydrolyze, was still observed in the XPS results as seen in Figure 2. This is probably due to the slow kinetics of the hydrolysis reaction of Li_2S and that the formation of LiOH consumes most of the water content.

Minor features suggest that also other degradation products can be observed in the XPS results. These features are located at 163.7 eV (polysulfur or polysulfide) and 160.5 eV in the S2p

spectrum for the graphite surface. The peak at 160.5 eV is assigned to be Li_2S since the position is in the range for metal sulfides[50] and Li_2S is one of the decomposition products according to the proposed mechanisms above. In summary, we can therefore propose a novel possible degradation mechanism for LiTFSI salt on graphite electrodes in SPE-based graphite half-cell based on our observations:

$$LiN(SO_2CF_3)_2 + ne^- + nLi^+ \rightarrow aLi_3N + bLiF + cLi_2S + dLi_2SO_3 + eS_z + fC_2F_xLi_y$$

According to Figure 3(a) and (b), more severe salt degradation could be found on the graphite electrode surfaces rather than on the SPE(G) surfaces. This observation can be due to the active lattice defects on the surface of graphite particles, which may catalyze the salt decomposition. Week signals at binding energies lower than 284 eV can be found in the C1s spectrum for the graphite sample surfaces, which are related to lithiated graphite species: Li_xC. The low intensity indicates that the measurement spot was a lithiated graphite particle covered by a thick SEI layer consisting of SPE residues, LiOH and various salt decomposition products. The week F1s signal at 688.7 eV corresponding to the Kynar binder further support such a conclusion.

Although SEI formation on graphite surfaces in liquid electrolyte LIBs have been intensively investigated in the past, the battery surface chemistry is here studied using the same LiTFSI salt in EC/DEC carbonate based electrolyte in order to obtain a systematic comparison. Salt residues are found on the liquid electrolyte battery graphite electrode even after the washing process, although the relative amount is quite low (N: 1.17%, S: 1.74%) according to Table 2. Here, the salt is found to be stable after the first discharge since both the S2p and N1s spectra are still dominated by pristine salt peaks and only negligible amount of LiF is detected. This is thus significantly different from the SPE batteries, where severe salt degradation was observed regardless of the water content.

The Li/SPE interface. The XPS results of the samples related to the Li/SPE interfaces are presented in Figure 4. The samples are, from top to bottom: 1) pristine Li, 2) pristine SPE, 3-6) Li and SPE(Li) surfaces from the two disassembled graphite half-cells with high (3-4) and low (5-6) H_2O content, and 7) Li electrode from the liquid electrolyte based graphite half-cell. The surface of the pristine lithium foil consists of only O, C and Li according to the XPS spectra in Figure 4 and the calculated atomic concentrations (in Table S1). The O1s spectrum for the lithium foil displays a dominant peak at 531.6 eV due to the presence of carbonate species, most likely to be Li_2CO_3. Moreover, a week signal at 528.3 eV is attributed to Li_2O. The C1s peak at 290 eV confirms the existence of Li_2CO_3 and another strong C1s peak at 285 eV originates from various hydrocarbon species. These compounds are commonly observed on metal lithium foils stored in the battery glovebox due to the high reactivity of the lithium surface. Here, the lithium foils were used as received.

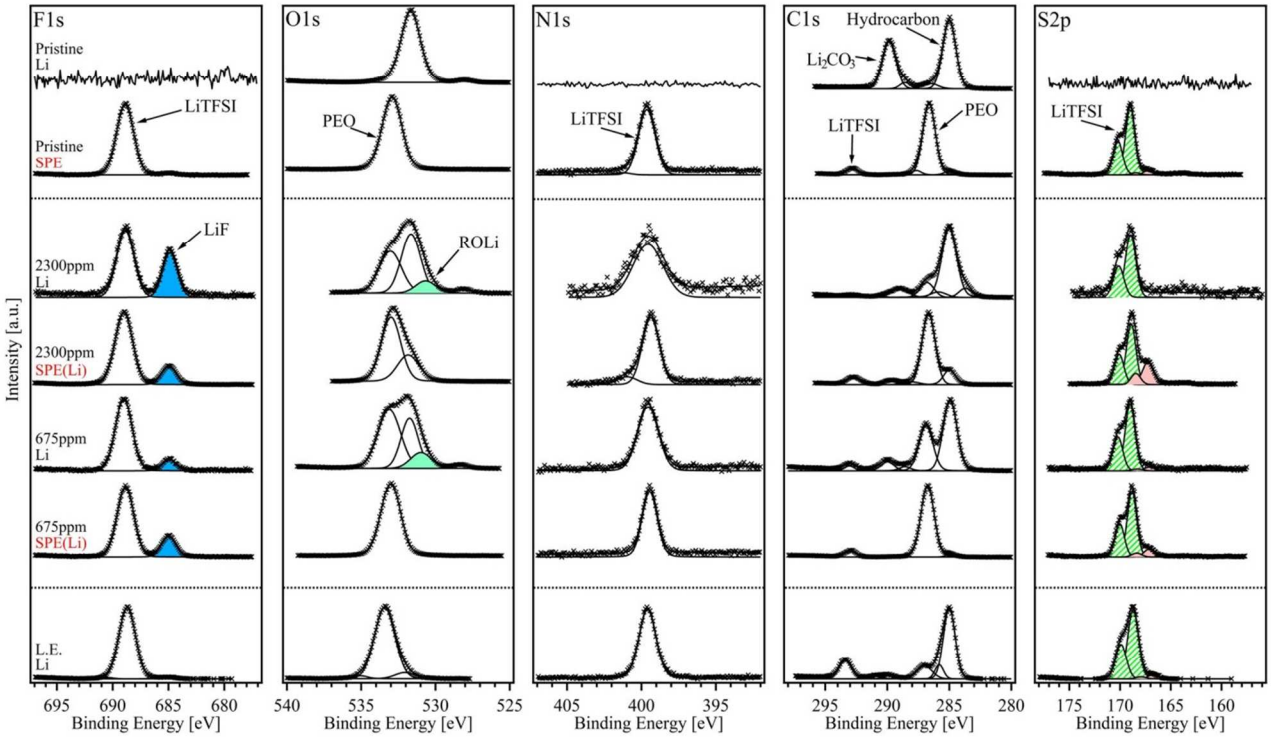

Figure 4. F1s, O1s, N1s, C1s, S2p spectra of pristine Li and SPE, Li and SPE(Li) from both SPE-based graphite half-cells (with different water content) and the lithium electrode from liquid electrolyte (L.E.) battery. Highlighted with difference colors are: LiF (blue), ROLi (light green), LiTFSI (green-patterned), and Li_2SO_3 (pink).

The cycled samples contain similar components as the pristine metal foil; Li_2O (O1s peak at 528 eV), hydrocarbon compounds and carbonate species, such as alkylcarbonate, lithium alkylcarbonate or lithium carbonate (O1s peaks at 531.6 eV), together with SPE residues. In addition to this, besides the some formation of LiF at the Li/SPE interface, the only new compound observed at this interface is lithium alkoxide species, ROLi, according to the presence of an O1s peak at 530.6 eV.[25]

This component is only observed on the Li side of the interface, indicating that ROLi is formed close to Li surface.

For the cycled samples, the N1s peaks and S2p peaks are all similar to the pristine sample and are dominated by the signals at 399.8 eV and 169 eV, respectively. In the S2p spectra for the SPE(Li) samples, there is a weak shoulder at 167.3 eV, originating from a sulfur-specie residue and can found in the pristine SPE sample as well. This finding shows that the salt is reasonably stable at this interface during the first discharge since no significant salt degradation observed. Thus, the SPE/Li interface layer mainly consists of the newly formed LiF, ROLi and pristine Li surface compounds together with SPE residues.

Overall, the composition of the SEI layer formed at the Li/SPE is significantly different from the one at the graphite/SPE interface, which consists of LiOH, LiF and salt degradation products such as Li_3N, Li_2S, S_x and Li_2SO_3. According to the XPS results presented here, the severe salt degradation found at the graphite side has little correspondence at the Li electrode. This is probably due to similar reasons for why more severe salt degradation was observed on the graphite surfaces rather than on the SPE(G) surfaces, correlated to that the defects on graphite may catalyze salt decomposition reactions.

In this context, the stability of LiTFSI salt in aqueous lithium ion battery systems has been investigated previously, and it was concluded that the salt show a favorable stability even at elevated temperature.[51] At the same time, however, $TFSI^-$ anions were found to be unstable in presence of water traces in ionic liquid systems.[52,53] It can thus not be ruled out that the salt decomposition observed in this study might also be due to the water content in the SPE, and not merely a catalytic reaction at the graphite surface.

Interestingly, although the electrode potential at the Li electrode is low enough for LiOH formation via water reduction, there was no LiOH detected at the Li/SPE interface. Our hypothesis is that the Li^+ ions and water molecules form aqua ion complexes $[Li(H_2O)_n]^+$, which will migrate from the Li electrode side to the graphite electrode during the 1st discharge. Therefore, the water is concentrated at the graphite/SPE interface and will be further reduced to produce LiOH.

In the spectra for the Li electrode from the liquid electrolyte cell, the signals of the natural surface species Li_2CO_3 and Li_2O have decreased. This indicates that there is a thick layer covering the Li foil even after washing with DMC. This passivation layer is found to exist of PEO-type polymer (O1s peak at 533 eV and C1s peak at 286.6 eV), hydrocarbons (C1s peak at 285 eV) and trace of salt residues, which are normally found for this type of cell.

Conclusions

The SEI formation in SPE-based graphite half-cells have been investigated by photoelectron spectroscopy technique and compared to conventional SEI formation in a liquid electrolyte cell in this study. In this context, we have also shown that the as-prepared PEO-based solid polymer electrolyte contains high water levels at hundreds of ppm. The water residue was found to be a key reactant for the intense LiOH production on the graphite electrode surface, where severe LiTFSI salt decomposition also was observed. At the Li/SPE interface, on the other hand, the newly produced species were dominated by lithium fluoride and lithium alkoxides. The significant difference in water content between the SPE films showed no distinct effect on the SEI compositions at either the Li/SPE or the graphite/SPE interfaces. However, obvious differences are observed in comparison with the conventional SEI formation in the LiTFSI-based liquid electrolyte cell where mainly decomposition products such as carbonate species, PEO-type polymer, etc, could be found. Figure 5 summarizes the obtained results and presents a schematic view of the compositions of the formed SEI layers after the first battery discharge.

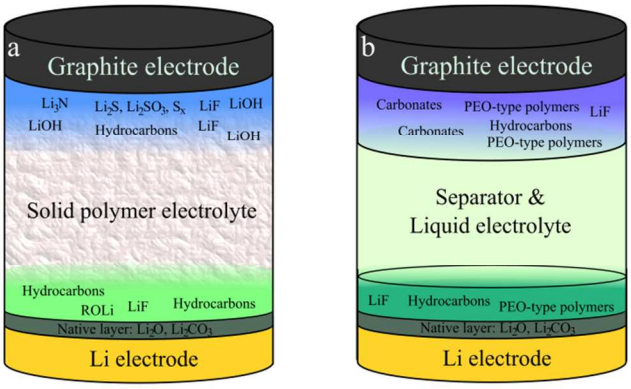

Figure 5. Schematic representation of the compositions of the SEI layers formed in (a) SPE-based and (b) conventional liquid electrolyte-based graphite half-cells.

These results indicate that the performance of SPE-based LIBs might be similarly controlled by the kinetics of the SEI layer, as is the case for liquid electrolyte systems. Hopefully, this study opens the door for future studies of the electrode/electrolyte interfacial chemistry in SPE-based LIBs, not least studies of conventional composite electrodes.

Acknowledgements

This research has been financed by the Swedish Research Council and the STandUP for Energy programme as well as the Swedish Energy Agency (STEM). DB wishes to thank the Carl Trygger Foundation for financial support.

Notes and references

Department of Chemistry – Ångström Laboratory, Uppsala University, Box 538, SE-751 21, Uppsala, Sweden. Email: daniel.brandell@kemi.uu.se; Fax: +46 18 513548; Tel: +46 18 4713709

† Electronic Supplementary Information (ESI) available: [details of any supplementary information available should be included here]. See DOI: 10.1039/b000000x/

1 B. Dunn, H. Kamath, and J.-M. Tarascon, *Science*, 2011, **334**, 928.
2 M. Armand and J.-M. Tarascon, *Nature*, 2008, **451**, 652.
3 Y. A. Samad, A. Asghar, and R. Hashaikeh, *Renew. Energy*, 2013, **56**, 90.
4 J. M. Tarascon and M. Armand, *Nature*, 2001, **414**, 359.
5 D. T. Hallinan and N. P. Balsara, *Annu. Rev. Mater. Res.*, 2013, **43**, 503.
6 A. Manuel Stephan and K. S. Nahm, *Polymer*, 2006, **47**, 5952.
7 W. Krawiec, L. G. Scanlon, J. P. Fellner, R. A. Vaia, S. Vasudevan, and E. P. Giannelis, *J. Power Sources*, 1995, **54**, 310.
8 F. Croce, G. B. Appetecchi, L. Persi, and B. Scrosati, *Nature*, 1998, **394**, 456.

9 E. F. Voronin, V. M. Gun'ko, N. V Guzenko, E. M. Pakhlov, L. V Nosach, R. Leboda, J. Skubiszewska-Zieba, M. L. Malysheva, M. V Borysenko, and A. A. Chuiko, *J. Colloid Interface Sci.*, 2004, **279**, 326.
10 H.-M. Xiong, Z.-D. Wang, D.-P. Xie, L. Cheng, and Y.-Y. Xia, *J. Mater. Chem.*, 2006, **16**, 1345.
11 H. S. Lee, X. Q. Yang, J. McBreen, Z. S. Xu, T. A. Skotheim, and Y. Okamoto, *J. Electrochem. Soc.*, 1994, **141**, 886.
12 M. S. Michael, M. M. E. Jacob, S. R. S. Prabaharan, and S. Radhakrishna, *Solid State Ionics*, 1997, **98**, 167.
13 P. P. Soo, B. Huang, Y. Jang, Y. Chiang, D. R. Sadoway, and A. M. Mayes, *J. Electrochem. Soc.*, 1999, **146**, 32.
14 Z. Zhang, D. Sherlock, R. West, R. West, K. Amine, and L. J. Lyons, *Macromolecules*, 2003, **36**, 9176.
15 A. Ghosh, C. Wang, and P. Kofinas, *J. Electrochem. Soc.*, 2010, **157**, A846.
16 G. T. Kim, G. B. Appetecchi, M. Carewska, M. Joost, a. Balducci, M. Winter, and S. Passerini, *J. Power Sources*, 2010, **195**, 6130.
17 M. C. Orilall and U. Wiesner, *Chem. Soc. Rev.*, 2011, **40**, 520.
18 B. Sun, I.-Y. Liao, S. Tan, T. Bowden, and D. Brandell, *J. Power Sources*, 2013, **238**, 435.
19 M. J. Smith, M. M. Silva, S. Cerqueira, and J. R. MacCallum, *Solid State Ionics*, 2001, **140**, 345.
20 B. Sun, J. Mindemark, K. Edström, and D. Brandell, *Solid State Ionics*, 2013, DOI: 10.1016/j.ssi.2013.08.014.
21 E. Peled, *J. Electrochem. Soc.*, 1979, **126**, 2047.
22 J. B. Goodenough and Y. Kim, *Chem. Mater.*, 2010, **22**, 587.
23 D. Aurbach, *J. Power Sources*, 2000, **89**, 206.
24 A. M. Andersson and K. Edström, *J. Electrochem. Soc.*, 2001, **148**, A1100.
25 A. M. Andersson, A. Henningson, H. Siegbahn, U. Jansson, and K. Edström, *J. Power Sources*, 2003, **119-121**, 522.
26 P. Verma, P. Maire, and P. Novák, *Electrochim. Acta*, 2010, **55**, 6332.
27 M. C. Smart, *J. Electrochem. Soc.*, 1999, **146**, 3963.
28 D. Ostrovskii, F. Ronci, B. Scrosati, and P. Jacobsson, *J. Power Sources*, 2001, **94**, 183.
29 S. Leroy, F. Blanchard, R. Dedryvère, H. Martinez, B. Carré, D. Lemordant, and D. Gonbeau, *Surf. Interface Anal.*, 2005, **37**, 773.
30 R. Dedryvere, S. Leroy, H. Martinez, F. Blanchard, D. Lemordant, and D. Gonbeau, *J. Phys. Chem. B*, 2006, **110**, 12986.
31 A. Nytén, M. Stjerndahl, H. Rensmo, H. Siegbahn, M. Armand, T. Gustafsson, K. Edström, and J. O. Thomas, *J. Mater. Chem.*, 2006, **16**, 3483.
32 D. Ensling, M. Stjerndahl, A. Nytén, T. Gustafsson, and J. O. Thomas, *J. Mater. Chem.*, 2009, **19**, 82.
33 B. Philippe, R. Dedryvère, M. Gorgoi, H. Rensmo, D. Gonbeau, and K. Edström, *Chem. Mater.*, 2013, **25**, 394.
34 E. Peled, D. Golodnitsky, G. Ardel, and V. Eshkenazy, *Electrochim. Acta*, 1995, **40**, 2197.
35 E. Peled, *J. Electrochem. Soc.*, 1997, **144**, L208.
36 M. Le Granvalet-Mancini, T. Hanrath, and D. Teeters, *Solid State Ionics*, 2000, **135**, 283.
37 I. Ismail, A. Noda, A. Nishimoto, and M. Watanabe, *Electrochim. Acta*, 2001, **46**, 1595.
38 C. L. Campion, W. T. Li, and B. L. Lucht, *J. Electrochem. Soc.*, 2005, **152**, A2327.
39 T. Kawamura, S. Okada, and J. Yamaki, *J. Power Sources*, 2006, 156, 547.
40 S. Scaccia, *Talanta*, 2005, **67**, 678.
41 S. K. Fullerton-Shirey, L. V. N. R. Ganapatibhotla, W. Shi, and J. K. Maranas, *J. Polym. Sci. Part B Polym. Phys.*, 2011, **49**, 1496.
42 K. Xu, *Chem. Rev.*, 2004, **104**, 4303.
43 A. M. Andersson, M. Herstedt, A. G. Bishop, and K. Edström, *Electrochim. Acta*, 2002, **47**, 1885.
44 D. Aurbach and I. Weissman, *Electrochem. commun.*, 1999, **1**, 324.
45 M. B. Armand, M. J. Duclot, and P. Rigaud, *Solid State Ionics*, 1981, **3–4**, 429.
46 F. M. Gray, Polymer Electrolytes, Royal Society of Chemistry, Cambridge, 1997, pp. 34–36.
47 Nakayama, S. Wada, S. Kuroki, and M. Nogami, *Energy Environ. Sci.*, 2010, **3**, 1995.
48 N. H. Turner, J. S. Murday, and D. E. Ramaker, *Anal. Chem.*, 1980, **52**, 84.
49 D. Aurbach, A. Zaban, Y. Ein-Eli, I. Weissman, O. Chusid, B. Markovsky, M. Levi, E. Levi, A. Schechter, and E. Granot, *J. Power Sources*, 1997, **68**, 91.
50 B. J. Lindberg, K. Hamrin, G. Johansson, U. Gelius, A. Fahlman, C. Nordling, and K. Siegbahn, *Phys. Scr.*, 1970, **1**, 286.
51 S. F. Lux, L. Terborg, O. Hachmöller, T. Placke, H.-W. Meyer, S. Passerini, M. Winter, and S. Nowak, *J. Electrochem. Soc.*, 2013, **160**, A1694.
52 P.C. Howlett, E.I. Izgorodina, M. Forsyth and D.R. MacFarlane, *Zeitschrift für Physikalische Chemie,* 2009, **220(10),** 1483.
53 S. Randström, M. Montanino, G. B. Appetecchi, C. Lagergren, A. Moreno, and S. Passerini, *Electrochim. Acta,* 2008, **53**, 6397.

Table of contents entry

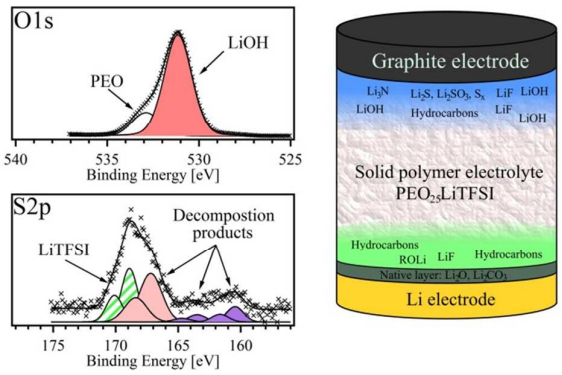

O1s and S2p XPS spectra of the graphite electrode after 1st discharge and schematic representation of the solid electrolyte interface (SEI) layers formed in an SPE-based graphite half-cell